

Dear Bouillon,

Thank you for your positive reply. Below is a response to your minor suggestion. We have also uploaded the final version of this manuscript along with all of the original figures.

A final minor suggestion: In response to Ref#1, you added a sentence mentioning that C/N ratios and $\delta^{15}\text{N}$ should be interpreted with caution "based on this pre-treatment method", I suggest you specify what type of bias (magnitude, direction) has been reported in the paper you cite.

We agree and have modified this sentence to read, Line 120-121: "The $\delta^{15}\text{N}$ results and the C/N ratios results should be interpreted with caution, based on this pre-treatment method, which may be influenced by the composition of the bulk organic matter (Brodie et al. 2011)."

1 **Historic carbon burial spike in an Amazon floodplain lake linked to riparian**
2 **deforestation near Santarem, Brazil**
3
4
5
6
7

8 Luciana M. Sanders¹, Kathryn Taffs¹, Debra Stokes², Christian J. Sanders³, Alex Enrich-
9 Prast^{4,5}, Leonardo Nogueira Amora^{6,7}, Humberto Marotta^{6,7}

10
11 ¹*School of Environment, Science and Engineering, Southern Cross University, Coffs Harbour, New South*
12 *Wales, Australia.*

13 ²*Marine Ecology Research Centre, Southern Cross University, P.O. Box 157, Lismore, NSW 2480, Australia*
14 *University, P.O. Box 157, Lismore, NSW 2480, Australia*

15 ³*National Marine Science Centre, School of Environment, Science and Engineering, Southern Cross*
16 *University, Coffs Harbour, New South Wales, Australia..*

17 ⁴*Laboratório de Biogeoquímica, Universidade Federal do Rio de Janeiro (UFRJ), Rio de Janeiro (RJ),*
18 *21941 971, Brazil.*

19 ⁵*Department of Environmental Change, Linköping University, 581 83, Linköping, Sweden.*

20 ⁶*Ecosystems and Global Change Laboratory (LEMG-UFF) / International Laboratory of Global Change*
21 *(LINCGlobal). Biomass and Water Management Research Center (NAB-UFF). Graduated Program in*
22 *Geosciences (Environmental Geochemistry). Universidade Federal Fluminense (UFF), Av. Edmundo*
23 *March, s/nº – Zip Code: 24210-310, Niteroi/RJ- Brazil.*

24 ⁷*Sedimentary and Environmental Processes Laboratory (LAPSA-UFF). Department of Geography.*
25 *Graduated Program in Geography. Universidade Federal Fluminense (UFF), Av. Gal. Milton Tavares*
26 *de Souza, s/nº - Zip Code: 24210-346, Niteroi/RJ- Brazil.*

27
28 *Corresponding author. E-mail address; l.sanders.13@student.scu.edu.au
29
30
31
32
33

34 **Abstract**

35 Forests along the Amazon Basin produce significant quantities of organic material, a
36 portion of which is deposited in floodplain lakes. Deforestation in the watershed may then have
37 potentially important effects on the carbon fluxes. In this study, a sediment core was extracted
38 from an Amazon floodplain lake to examine the relationship between carbon burial and
39 changing land cover/land use. Historical records from the 1930s and satellite data from the
40 1970s were used to calculate deforestation rates between 1930 and 1970, and 1970 to 2010 in
41 four zones with different distances from the margins of the lake and its tributaries (100, 500,
42 1000 and 6000 m buffers). A sediment accumulation rate of $\sim 4 \text{ mm year}^{-1}$ for the previous ~ 120
43 years was determined from the $^{240+239}\text{Pu}$ signatures and the excess ^{210}Pb method. The carbon
44 burial rates ranged between 85 and 298 $\text{g C m}^{-2} \text{ year}^{-1}$, with pulses of high carbon burial in the
45 1950s, originating from the forest vegetation as indicated by $\delta^{13}\text{C}$ and $\delta^{15}\text{N}$ signatures. Our
46 results revealed a potentially important spatial dependence of the OC burial in Amazon
47 lacustrine sediments in relation to deforestation rates in the catchment. These deforestation
48 rates were more intense in the riparian vegetation (100 m buffer) during the period 1930 to
49 1970 and the larger open water areas (500, 1000 and 6000 m buffer) during 1970 to 2010. The
50 continued removal of vegetation from the interior of the forest was not related to the peak of
51 OC burial in the lake, but only the riparian deforestation which peaked during the 1950s.
52 Therefore, this supports the conservation priority of riparian forests as an important
53 management practice for Amazon flooded areas. Our findings suggest the importance of abrupt
54 and temporary events in which some of the biomass released by the deforestation, especially
55 restricted to areas along open water edges, might reach the depositional environments in the
56 floodplain of the Amazon Basin.

57

58

59 **1. Introduction**

60 Rivers act as vectors, transporting sediment from land to ocean (Abril et al. 2014). Along
61 this trajectory a significant proportion of the sediment load, including organic material, may be

62 deposited in floodplains, creating zones of carbon accumulation (Smith et al. 2002, Dong et al.
63 2012, Hoffmann et al. 2013). This process is accelerated during flood events, when rivers and
64 tributaries deposit organic material along the inundated floodplains (Smith et al. 2002). In some
65 climate zones, floodplains are seasonally inundated, with riparian zone vegetation dependent
66 upon this seasonal influx of organic material. The riparian vegetation slows water velocity and
67 traps fine-grained, carbon rich sediments within this low-energy environment (Aalto et al.
68 2003). Therefore, the riparian vegetation along the floodplains may be important for the organic
69 matter deposition and the Amazon carbon cycle.

70 The importance of tropical wetland ecosystems in the carbon cycle is well documented
71 (Downing et al. 1993, Melack et al. 2004, Zocatelli et al. 2013, Abril et al. 2014, Marotta et al.
72 2014). It has been shown that wetlands in the warm tropics are some of the most productive
73 biological communities in the world (Neue et al. 1997), representing an important sink for
74 nutrients (Marotta et al. 2009) and carbon (Peixoto et al. 2016, Sanders et al. 2017), as well as
75 sources of organic substrates to carbon gas production in inland waters (Marotta et al. 2010).
76 However, these wetland ecosystems are also highly threatened by land use activities, especially
77 from deforestation, development of agricultural land and soil degradation (Junk 2013, Lucas et
78 al. 2014).

79 The Amazon Basin wetlands are being degraded by farming activities such as commercial
80 ranching and an increase in road density (Goulding 1993). Deforestation of the Amazon Basin
81 commenced ~ 1930 and accelerated toward the end of the 1970's (Skole and Tucker 1993),
82 when an estimated 15% of the pristine rainforest area was lost by the year 2003, increasing to
83 approximately 18% by 2015 (INPE 2016). The ongoing loss of vegetation is responsible for a
84 substantial increase in erosion rates and subsequent sediment inputs into Amazon rivers and
85 lakes (Neill et al. 2013b). Yet these anthropogenic activities are potential sources of

86 allochthonous organic matter that may increase carbon stores in the associated floodplain areas
87 (Diaz and Rosenberg 2008, Stanley et al. 2012).

88 Jupindá Lake, in the state of Pará, provides an ideal opportunity to investigate historical
89 changes in organic carbon burial in a floodplain lake as a result of the well documented
90 anthropogenic activities within its watershed. This will aid in identifying the little known
91 impacts of land cover changes on recent carbon burial rates in depositional environments of
92 the Amazon floodplain. The objectives of this research are to investigate the effects of
93 deforestation and urban development on carbon burial rates in a tropical floodplain lake. We
94 hypothesize that the historical deforestation in this region of the Amazon may have influenced
95 the OC burial rates in the studied floodplain lake.

96

97 **2. Methods**

98 The city of Santarém, in central Amazon, was established in the mid-eighteenth century,
99 approximately 650 km upstream from the Amazon River mouth and at its confluence with the
100 Tapajós River (02°25'0.28"S and 54°42'41.57"W, Figure 1). In 1940, Santarém was only a
101 small village, less than 0.5 km², surrounded by dense pristine rainforest (estimated from the
102 historical mapping of the Santarém City Hall). This city quickly expanded, occupying 5.2 km²
103 by the end of the 1970s and 49.3 km² currently (estimated from satellite images
104 LANDSAT/SRTM). Jupindá Lake is 70 km east of Santarém City, and receives surface water
105 inflow from small streams draining from the forest and the main tributary Curuá-Una River, a
106 large affluent of the Amazon River (Figure 1). The Lake has been affected by the deforestation
107 associated with the expansion of Santarém City. Between the 1940's and 1950's, there was
108 intense deforestation on the margins of rivers and streams in this area, used to supply the
109 markets with wood and forestry products (Amorim 2000, Cruz et al. 2011). In the 1970s, the

110 Curuá-Una River was dammed (Curuá-Una Dam) 45 km upstream of Jupindá Lake to build
111 the first hydroelectric plant of the Amazon Forest (Ligocki 2003).

112 A 60 cm sediment core (diameter 7.5 cm) was collected in 2010 using a gravity corer in the
113 center of the Jupindá Lake (02°27'43.60" S, 54° 5'1.30" W). The sediment core was sub
114 sampled at 2 cm intervals. Dry bulk density (DBD, g cm^{-3}) was determined as the dry sediment
115 weight (g) divided by the initial volume (cm^3). A homogenized portion was acidified (10%
116 HCl following the procedures outlined in Naidu et al. (2000)) to remove carbonate material,
117 then dried and ground to powder for organic carbon (OC), nitrogen (N), $\delta^{13}\text{C}$, and $\delta^{15}\text{N}$ analyses
118 using a Flash Elemental Analyzer coupled to a Thermo Fisher Delta V IRMS (isotope ratio
119 mass spectrometer). The $\delta^{15}\text{N}$ results and the C/N ratios results should be interpreted with
120 caution, based on this pre-treatment method, which may be influenced by the composition of
121 the bulk organic matter (Brodie et al. 2011). Working standards were used (glucose, 10.7 ppt
122 and urea, 41.3 ppt) to calibrate for $\delta^{13}\text{C}$. A pair of standards was measured with every 20
123 samples. These standards were calibrated initially against international absolute standards
124 LSVEC and NIST8542. Analytical precision: C = 0.1 %, N = 0.1%, $\delta^{13}\text{C}$ = 0.1‰ and $\delta^{15}\text{N}$ =
125 0.15 ‰.

126 Samples were prepared for Pu dating following the method of Ketterer et al. (2004) with
127 modifications to enable larger sample mass to be processed as a result of the likely lower Pu
128 concentrations in the Southern Hemisphere (Sanders et al. 2016). To obtain a larger mass,
129 sediment intervals were joined and homogenized so the sediment intervals for the $^{240+239}\text{Pu}$
130 dating was 4 cm intervals. Sample aliquots ranging from 14 to 29 grams were dry-ashed at 600
131 °C for 16 hours, and leached with 50 mL of 16 M HNO_3 . The leaching was conducted overnight
132 at 80°C with added ^{242}Pu yield tracer (NIST 4334g, 19 picograms). Acid leaching (as opposed
133 to complete dissolution with HF) is known to solubilize stratospheric fallout Pu, and there is
134 little possibility that “refractory” HNO_3 -insoluble Pu exists in the South America (Sanders et

135 al. 2014). The leachates were diluted to 100 mL, filtered to remove solids, and the aqueous
136 solutions were processed with TEVA resin (EiChrom, Lisle, IL, USA) in order to chemically
137 isolate 3.0 mL Pu fractions in aqueous ammonium oxalate solution suitable for measurements
138 by sector ICPMS. Pu determinations were performed using a VG Axiom MC operating in the
139 single collector (electron multiplier) mode. The system was used with an APEX HF desolvating
140 micronebulizer system (ESI Scientific, Omaha, NE, USA) with an uptake rate of 0.4
141 mL/minute. Qualitative mass spectral scans (averages of 50 sweeps over the mass range 237.4
142 – 242.6) were collected for selected samples prior to the electrostatic sector quantitative
143 scanning of $^{238}\text{U}^+$, $^{239}\text{Pu}^+$, $^{240}\text{Pu}^+$, and $^{242}\text{Pu}^+$. Detection limits were evaluated based upon the
144 analysis of two blanks and considerations regarding the obtained mass spectra. A detection
145 limit of 0.01 Bq/kg of $^{239+240}\text{Pu}$ is applicable for samples of nominal 25 g mass.

146 For ^{210}Pb dating, an intrinsic germanium detector coupled to a multi-channel analyzer was
147 used. Freeze dried and ground sediments were packed and sealed in gamma tubes. Lead-210
148 and ^{226}Ra activities were calculated by multiplying the counts per minute by a factor that
149 includes the gamma-ray intensity and detector efficiency determined from standard
150 calibrations. Identical geometry was used for all samples. Lead-210 activities were determined
151 by the direct measurement of the 46.5 KeV gamma peak. Radium-226 activity was determined
152 via the ^{214}Pb daughter at 351.9 KeV. For ^{226}Ra measurements, the packed samples were set
153 aside for at least 21 days to allow for ^{222}Rn to ingrow and establish secular equilibrium between
154 ^{226}Ra and its granddaughter ^{214}Pb . Excess ^{210}Pb activity was calculated by subtracting the
155 supported ^{210}Pb (i.e., ^{226}Ra activity) from the total ^{210}Pb activity. The sediment accretion rate
156 for the previous 120 years was estimated by two methods derived from ^{210}Pb dating, the
157 Constant Initial Concentration (CIC) model assuming that this rate has not varied during the
158 encompassed time span (Appleby and Oldfield 1992), and the Constant Rate of Supply (CRS)
159 model based on a constant influx of unsupported, atmospheric ^{210}Pb that allows a variable

160 sediment rate (Ivanovich and Harmon 1992). Organic carbon accumulation rates were
161 estimated from an average between these the two dating methods ($^{239+240}\text{Pu}$ and $^{210}\text{Pb}_{\text{ex}}$), the
162 dry bulk density (g cm^3) and carbon content for each interval of the entire sediment core.

163 The land use and land cover analysis was based on documented historical information
164 before 1975 and satellite images (Landsat/SRTM, Table 1) from 1975, 1985, 1995 and 2008
165 available from the United States Geological Survey (USGS). No significant deforestation
166 occurred in the catchment area of the Jupindá Lake until the early 1940's (Amorim 2000, Cruz
167 et al. 2011). Subsequent land/use changes were determined using satellite images (Gordon
168 1980, Munyati 2000). All satellite images were from low-water seasons to remove the influence
169 of the flood pulse on the exposed area over years. The resolution of the images was 30 m,
170 except that from the 1970's, which was resampled from 90 to 30 m (Table 1). This approach
171 allowed an assessment of changes in land cover could then be compared to results from carbon
172 accumulation. Results of the spatial assessment were separated into two time periods; 1930 to
173 1970, the timeframe between the onset of land clearing and the first satellite image, and 1970
174 to 2010 which provides a more detailed assessment of temporal changes to the study area. The
175 time period 1930 to 1970 was characterized by a rapid removal (peak until the 1960's) of
176 vegetation established at the margins of inland waters; especially *Aniba rosaeodora* (Pau-rosa)
177 for extraction of oils, and *Mezilaurus itauba* and *Cedrela fissilis* (Louro-itaúba and Cedro,
178 respectively) as hardwoods, and the opening of clearings for crops of textile fibers and
179 subsistence products. Intensification of deforestation towards the interior of the forest and
180 following the urban growth of Santarém is reported from the 1970's (Amorim 2000, Cruz et
181 al. 2011). The depletion of vegetation near to the margins of lakes and running waters in this
182 region is also well documented (Amorim 2000, Cruz et al. 2011).

183 In order to address the spatial dependence of recent OC burial in Jupindá Lake for
184 deforestation, we analyzed the land cover and land use in four buffer areas around the lake and

185 contributing rivers or streams. The first buffer of 100 m represented the riparian forest protected
186 area by the Brazilian laws for fluvial channels with a width of 50 to 200 m. Other buffers were
187 progressively higher, with a width of 500, 1000 and 6000 m from the riverbank and lake
188 margins (Figure 2). In addition, we considered only stretches of rivers and streams 65 km long
189 from Jupindá Lake to analyze its catchment area of more direct influence. This criteria also
190 avoids the interference of the artificial flooding on the margins of the Curuá-Una hydroelectric
191 dam, which was built in 1977 (Fearnside 2005).

192 The statistical treatment of variables and OC burial rates, when grouped into different
193 phases, showed assumptions which required parametric analyses, including normal
194 distribution (Kolmogorov-Smirnov, $p > 0.05$) and homogeneity of variance (Bartlett, $p > 0.05$).
195 Thus, we used means and standard errors to represent the distribution of values, and parametric
196 tests were conducted, allowing comparison of different phases. Statistical differences were
197 tested using the one-way ANOVA test followed by Tukey's post test (significance was defined
198 as $p < 0.05$). All the statistical tests used in this work were performed using GraphPad Prism
199 5.0 software.

200

201 3. Results

202 The analyses of $^{239+240}\text{Pu}$ showed no detectable activities from the base of the sediment core
203 until the 22-26 cm interval (Figure 3). However, $^{239+240}\text{Pu}$ was detected in the 18-22 cm interval
204 ($0.029 \pm 0.002 \text{ Bq/kg } ^{239+240}\text{Pu}$) with the peak concentration ($0.047 \pm 0.004 \text{ Bq/kg } ^{239+240}\text{Pu}$) at
205 the 16 cm depth, which indicates the 1963 stratospheric fallout peak. Hence material below 22
206 cm was deposited pre-bomb (that is, prior to the early 1950's). This affixes an upper limit on
207 the average sedimentation rate of near to 3.8 mm year^{-1} . The Pu atom ratio data indicate that
208 the Pu is originating from stratospheric fallout with isotopic ratios ($^{240/239}\text{Pu}$) of ~ 0.18 . These
209 results are consistent with the $^{240}\text{Pu}/^{239}\text{Pu}$ of 0.180 ± 0.014 discussed by Kelley et al. (1999).

210 The ^{210}Pb and ^{226}Ra profiles as well as the $^{210}\text{Pb}_{\text{(ex)}}$ profile vs cumulative dry mass
211 accumulation reveals a complex depositional environment with sedimentation variations and
212 disturbances, such as bioturbation and resuspension in the upper ~ 20 cm of the sediment
213 column (Figure 4). A decrease in $^{210}\text{Pb}_{\text{ex}}$ activity was found below the 20 cm depth interval.
214 The $^{210}\text{Pb}_{\text{ex}}$ data distribution are as follows: $y = -0.0749x + 7.5$; $R^2 = 0.73$; $n=19$; $p < 0.01$ from
215 the 20 to the 60 cm interval, below the apparent mixed zone. Both estimates of sediment
216 accretion rate during the 120 years from CIC and CRS models were similar, reaching 4.1 and
217 4.3 mm yr^{-1} respectively, which were slightly higher than the ~ 60 year $^{239+240}\text{Pu}$ dates (3.8 mm
218 yr^{-1}). In order to obtain a more reliable estimates of the historical carbon burial rates, the
219 $^{239+240}\text{Pu}$ results, from near 1950 to present, were used (3.8 mm year^{-1}) and $^{210}\text{Pb}_{\text{ex}}$ (4.2 mm
220 year^{-1}) was used from ~1890 to approximately the 1950s. These rates for each sediment depth
221 were multiplied by the DBD and OC content for each interval of the entire sediment core.

222 The dry bulk density (DBD), total organic carbon (OC%), total nitrogen (TN%) content as
223 well as the carbon and nitrogen (C/N) molar ratios along with the $\delta^{13}\text{C}$ and $\delta^{15}\text{N}$ values showed
224 a decreasing shift towards the center of the sediment core (Table 2). The relationship between
225 $\delta^{13}\text{C}$ and $\delta^{15}\text{N}$ indicated different origins of OC in the sediment core (Figure 5) contributing to
226 the significant relationship between OC burial and the $\delta^{13}\text{C}$ (Figure 6). The significantly greater
227 $\delta^{13}\text{C}$ peak and lower $\delta^{15}\text{N}$ values coupled to higher OC burial rates were observed in the phase
228 between ~1930 to 1970 in Jupindá Lake (one-way ANOVA followed by Tukey's post test,
229 $p < 0.05$; Fig. 7). The $\delta^{13}\text{C}$ values were greater in the phase ~1930 to 1970 in relation to those
230 previous and after respectively (one-way ANOVA followed by Tukey's post test, $p < 0.05$). This
231 peak near 1950 also showed $\delta^{15}\text{N}$ values lower and OC burial rates higher than other
232 phases (one-way ANOVA followed by Tukey's post test, $p < 0.05$).

233 The OC burial rates indicate an increasing trend from ~ 1930 with a peak during the 1940's
234 and 50's (Figure 7). The carbon burial rates increased from ~ $186 \text{ g m}^{-2} \text{ year}^{-1}$ before the 1950s,

235 and up to 298 g m⁻² year⁻¹ between the 1940s and 1950s. Carbon accumulation then decreased
236 to approximately 186 g m⁻² year⁻¹ from 1960 to 1980, after which a gradual decline in carbon
237 burial is noted. In relation to land use/cover in the surrounding fluvial channels and the Jupindá
238 Lake, only the smallest buffer (100 m) showed significant changes during 1930-1970. This
239 time period is when deforestation was nearly 75% higher than in the subsequent time period
240 1970-2010 (Figure 8a) and when OC burial was greatest (Figure 8b).

241

242 **4. Discussion**

243 Similar estimates of sediment accretion were calculated using different methodologies
244 (²³⁹⁺²⁴⁰Pu and ²¹⁰Pb_(ex)). These accretion rates along with the dry bulk density revealed an
245 insight into changes in the sediment sources of floodplains, and their relationships with
246 changing land cover and land use in the Amazon Basin. The Jupindá Lake showed substantial
247 changes in the carbon burial rates following deforestation, supporting the connection between
248 flooded areas and their surrounding vegetation. The high peak in carbon accumulation observed
249 around 1950 appears to be associated with a shift in the source of organic material, inferred by
250 changes in carbon and nitrogen contents and the isotopic fractioning toward the middle (from
251 20 to 40 cm depth interval) of the sediment column. This peak for different organic and
252 inorganic variables in intermediate depths revealed changes not only in the amount but also in
253 the type of material being deposited over time. Previous studies have reported two common
254 origins for OC in the Amazon forest. Higher $\delta^{15}\text{N}$ and more negative $\delta^{13}\text{C}$ values could indicate
255 the presence of Santarém soil organic matter (such as that adjacent to the Jupindá Lake), while
256 lower $\delta^{15}\text{N}$ and more variable $\delta^{13}\text{C}$ values indicate particulate organic carbon (POC) from the
257 terrestrial vegetation in the catchment (Ometto et al. 2006, Zocatelli et al. 2013). Here, a
258 corresponding increase in OC%, TN% and OC burial rates measured, with a peak near 1950,
259 suggesting higher inputs of organic matter into lake. The higher $\delta^{13}\text{C}$ signature, coupled with a

260 lower $\delta^{15}\text{N}$ indicates a greater influence from the terrestrial Amazonian POC during the same
261 period, around 1950 (Ometto et al., 2006).

262 When looking for a cause for this change in the source of organic material, we look to the
263 analysis of land use change. Land clearing associated with early occupation from the 1940s in
264 the catchment area of the Jupindá Lake may be a potential cause of the increased carbon burial
265 observed in the lake. Changes in land use and associated deforestation may significantly affect
266 OC burial in mid-high-latitude lakes (Anderson et al. 2013, Dietz et al. 2015). Indeed, our
267 results suggest that land clearing during the 1940's and 50's might be related to increased
268 organic matter deposition in the region's floodplain lakes. During this period, intense wood
269 extraction and expansion of agricultural settlements occurred (Amorim 2000, Cruz et al. 2011).
270 One important consequence of deforestation in the watershed is the silting up of lakes (Enea et
271 al. 2012), including those at humid low-latitude areas (Cohen et al. 2005, Bakoariniaina et al.
272 2006). However, the lake is in a region relatively well protected, and therefore there is no other
273 explanation other than deforestation in the margins to have caused the peak in OC burial near
274 the 1950s. The riparian forest systems are generally effective in reducing the sediment transport
275 by surface runoff, with the removal of this vegetation increasing the erosion processes,
276 especially in the Amazon Basin as a result of intense rainfall (Neill et al. 2013a). The peak of
277 the significantly greater $\delta^{13}\text{C}$ and lower $\delta^{15}\text{N}$ values coupled to higher OC burial rates were
278 observed in the phase between ~1930 to 1970 in Jupindá Lake (one-way ANOVA followed by
279 Tukey's post test, $p < 0.05$; Fig. 7). The $\delta^{13}\text{C}$ values were greater in the ~1930 to 1970 phase as
280 related to those previous and after respectively (one-way ANOVA followed by Tukey's post
281 test, $p < 0.05$). This peak between ~1930 to 1970 also showed delta $\delta^{15}\text{N}$ values lower and OC
282 burial rates higher than other phases (one-way ANOVA followed by Tukey's post test,
283 $p < 0.05$).

284 We also found a spatial dependence of the carbon accumulation in Lake Jupindá, as the
285 much lower OC burial was coupled to higher deforestation rates in those larger buffers around
286 its margins and main fluvial channels (500, 1000 and 6000 m) in the period after 1970s
287 (between the 1970s to 2010) than that before (~1930 to 1970). This confirms previous evidence
288 that the recent deforestation process in the region commenced in the riparian zone (Amorim
289 2000, Cruz et al. 2011), and not in the interior of the forest. The enhanced OC burial in
290 lacustrine sediments before ~1970 was related to higher deforestation rates only in the riparian
291 vegetation zone (100 m buffers), suggesting a higher influence of deforestation with decreasing
292 distance to water courses. Therefore, the soil carbon enrichment to the aquatic sediments during
293 the peaks of riparian deforestation may cause intense but temporary carbon burial events in the
294 Amazon floodplain, representing potentially only a significant part of the total loss of terrestrial
295 organic matter. In addition, the continued removal of vegetation from the interior of the forest
296 might not be directly related to increases of OC burial, even temporarily, in depositional aquatic
297 ecosystems.

298

299 **5. Conclusion**

300 Palaeolimnological techniques were used with a historical spatial analysis of deforestation
301 to interpret changes in sediment characteristics during the past century. The Pu dating method
302 closely approximates measurements from the ^{210}Pb chronologies and hence offers a technique
303 to determine sedimentation rates and carbon accumulation in Amazon sediments. An increase
304 in OC burial, up to $298 \text{ OC g m}^{-2} \text{ year}^{-1}$, coincides with changes in the $\delta^{13}\text{C}$ and $\delta^{15}\text{N}$ signatures,
305 likely influenced by the heavy deforestation in riparian systems of this region during the 1940s
306 and 1950s. It is suggested that the net increase in carbon burial towards the center of the
307 sediment core, which represents the highest carbon burial rates during the 1950s, is a result of
308 a change in source of organic matter deposition. However, any increase of OC burial rates

309 attributed to deforestation might be lower than the loss of terrestrial biomass in the standing
310 crop or soils. The differing carbon burial rates along the sediment core therefore identify the
311 potential complexity of the Amazon floodplain lakes, directly related to the development within
312 the Basin. This work supports the urgent need for management practices based on the
313 conservation of riparian forests, demonstrating the spatial dependence of carbon burial capacity
314 of the Amazon floodplain lakes with respect to advances in deforestation in the Basin.

315

316 **Acknowledgements**

317 LMS is supported by an APA and IPRS scholarships. HM received a research grant from the
318 Brazilian Research Council (CNPq – “Programa Universal”) and the Research Support
319 Foundation of the State of Rio de Janeiro (FAPERJ – “Programa Jovem Cientista do Nosso
320 Estado”). CJS is supported by the Australian Research Council (DE160100443).

321

322

323 **CAPTIONS TO FIGURES**

324 **Figure 1.** Jupindá Lake where the sediment core was extracted, near the Amazon River and
325 the city of Santarém, Brazil. This floodplain lake has a diameter of approximately 3 km.

326 **Figure 2.** Different buffer sizes (100 m, 500 m, 1 km and 6 km) along the stretch of the
327 Curuá-Una River from Jupindá Lake (red) to the hydroelectric dam upstream (yellow).

328 **Figure 3.** $^{239+240}\text{Pu}$ profile, indicating ~ 1950 when these radionuclides were first introduced
329 into the atmosphere.

330 **Figure 4.** Lead-210 (black circles) and ^{226}Ra (white circles) profiles against depth. Grey
331 squares represent the $^{210}\text{Pb}(\text{ex})$ profile vs cumulative dry mass.

332 **Figure 5.** $\delta^{13}\text{C}$ vs $\delta^{15}\text{N}$. The Amazon River POM and Santarem soil organic matter values,
333 adjacent to the study area, are taken from Zocatelli et al (2013).

334 **Figure 6.** Carbon burial as a function of $\delta^{13}\text{C}$ and $\delta^{15}\text{N}$.

335 **Figure 7.** $\delta^{13}\text{C}$, $\delta^{15}\text{N}$ and carbon burial rate values in relation to depth (cm). Panels below
336 each vertical profile represent respective data grouped by the three general phases >1930,
337 1930-1970 and 1970-2010. Filled square symbols represent means of a given variable in
338 each sediment layer, and the vertical bars show the mean with the standard deviation of the
339 respective phase. Equal letters in each panel represent non-significant differences ($p > 0.05$,
340 one-way ANOVA followed by Tukey's post test).

341 **Figure 8.** Percentage of modified areas in relation to the different buffers (Panel A). Carbon
342 burial (black dots) and changes in the riparian vegetation (two grey bars represent the two
343 general phases) as related to time (Panel B).

344

345

346

347

348 **CAPTION TO TABLES**

349 **Table 1.** Satellite acquisition data from United States Geological Survey (USGS) and the
350 Curuá-Una River quota from Brazilian Water Agency (ANA).

351 **Table 2.** Depth profiles of dry bulk density (DBD), total organic carbon (OC%), total nitrogen
352 (TN%) carbon and nitrogen (C/N) molar ratios, $\delta^{13}\text{C}$ and $\delta^{15}\text{N}$.

353

354

355

356

357

358

359

360

361

362

363

364

365

366
 367
 368
 369
 370
 371
 372
 373
 374

Table 1.

<i>Month/Year</i>	<i>Landsat Data</i>	<i>Curuá-Una River Quote</i>
Aug/1975	2	5.3
Oct/1985	5	3.7
June/1995	5	6
June/2008	5	<i>No data</i>

375
 376
 377
 378
 379
 380
 381
 382

Table 2.

Depth (cm)	DBD (g cm⁻³)	δ¹⁵N	δ¹³C	C (%)	N (%)	C/N
0-2	1.0	8.9	-29.2	3.8	0.3	17.2
2-4	0.9	11.7	-29.0	3.8	0.3	18.7
4-6	1.0	10.4	-28.8	4.0	0.3	19.2
6-8	1.1	9.3	-28.7	4.3	0.3	20.2
8-10	1.0	9.4	-28.7	4.1	0.3	19.8
10-12	1.1	7.9	-28.6	4.6	0.3	21.2
12-14	1.1	8.2	-28.7	4.3	0.3	19.9
14-16	1.1	7.8	-28.6	4.3	0.3	20.9
16-18	1.0	8.7	-28.5	4.4	0.3	21.2
18-20	1.1	7.5	-28.4	4.4	0.3	19.8
20-22	1.0	6.5	-28.2	5.4	0.3	21.2
22-24	1.0	6.0	-27.8	5.3	0.3	21.5
24-26	1.0	5.2	-27.4	7.3	0.4	25.4
26-28	1.1	6.1	-27.6	6.0	0.3	23.8
28-30	1.0	5.0	-27.3	6.0	0.4	22.7
30-32	1.0	5.4	-28.0	6.1	0.3	27.0
32-34	1.3	6.6	-28.5	4.4	0.2	27.5
34-36	1.6	8.9	-29.0	2.2	0.1	23.1
36-38	1.4	11.4	-29.4	2.9	0.1	30.4
38-40	1.4	10.4	-29.5	3.3	0.1	30.5
40-42	1.5	11.4	-29.3	2.4	0.1	23.8
42-44	1.6	12.2	-29.4	1.3	0.1	15.6
44-46	1.8	8.2	-29.6	1.2	0.1	14.3
46-48	1.5	8.8	-29.8	2.2	0.1	21.6
48-50	0.9	10.4	-29.7	2.9	0.2	25.6
50-52	0.9	10.2	-29.7	2.6	0.1	27.2
52-54	0.9	7.1	-29.7	3.9	0.2	28.6
54-56	0.9	9.2	-29.9	3.6	0.2	27.8
56-58	0.9	6.6	-30.1	4.3	0.2	30.1

58-60	0.9	5.0	-30.1	3.5	0.2	23.1
Average	1.11	8.34	-28.9	4.0	0.2	23.0
Stand Dev	0.24	2.1	0.8	1.9	0.1	4.2

References

- 383
384
385 Aalto, R., L. Maurice-Bourgoin, T. Dunne, D. R. Montgomery, C. A. Nittrouer, and J. L.
386 Guyot. 2003. Episodic sediment accumulation on Amazonian flood plains influenced
387 by El Niño/Southern Oscillation. *Nature* **425**:493-497.
- 388 Abril, G., J. M. Martinez, L. F. Artigas, P. Moreira-Turcq, M. F. Benedetti, L. Vidal, T.
389 Meziane, J. H. Kim, M. C. Bernardes, N. Savoye, J. Deborde, E. L. Souza, P. Albéric,
390 M. F. Landim De Souza, and F. Roland. 2014. Amazon River carbon dioxide
391 outgassing fuelled by wetlands. *Nature* **505**:395-398.
- 392 Amorim, A. T. d. S. 2000. Santarém: uma síntese histórica, Canoas, Ulbra, Santarem, Brazil
- 393 Anderson, N. J., R. D. Dietz, and D. R. Engstrom. 2013. Land-use change, not climate,
394 controls organic carbon burial in lakes. *Proceedings. Biological sciences / The Royal*
395 *Society* **280**:20131278.
- 396 Appleby, P. G., and F. Oldfield. 1992. Application of lead-210 to sedimentation studies.
397 Pages 731-783 in M. Ivanovich and S. Harmon, editors. *Uranium Series*
398 *Disequilibrium: Application to Earth, Marine and Environmental Science*. Oxford
399 *Science Publications*.
- 400 Bakoariniaina, L. N., T. Kusky, and T. Raharimahefa. 2006. Disappearing Lake Alaotra:
401 Monitoring catastrophic erosion, waterway silting, and land degradation hazards in
402 Madagascar using Landsat imagery. *Journal of African Earth Sciences* **44**:241-252.
- 403 Brodie, C. R., J. S. L. Casford, J. M. Lloyd, M. J. Leng, T. Heaton, C. P. Kendrick, and Z.
404 Yongqiang. 2011. Evidence for bias in C/N, $\delta^{13}\text{C}$ and $\delta^{15}\text{N}$ values of bulk organic
405 matter, and on environmental interpretation, from a lake sedimentary sequence by
406 pre-analysis acid treatment methods. *Quaternary Science Reviews* **30**:3076-3087.
- 407 Cohen, A. S., M. R. Palacios-Fest, J. McGill, P. W. Swarzenski, D. Verschuren, R. Sinyinza,
408 T. Songori, B. Kakagozo, M. Syampila, C. M. O'Reilly, and S. R. Alin. 2005.
409 Paleolimnological investigations of anthropogenic environmental change in Lake
410 Tanganyika: I. An introduction to the project. *Journal of Paleolimnology* **34**:1-18.
- 411 Cruz, H., P. Sablayrolles, M. Kanashiro, and M. S. Amaral, P. 2011. Relação empresa/
412 comunidade no manejo florestal comunitário e familiar: Uma contribuição do Projeto
413 Floresta em pé.
- 414 Diaz, R. J., and R. Rosenberg. 2008. Spreading dead zones and consequences for marine
415 ecosystems. *Science* **321**:926-929.
- 416 Dietz, R. D., D. R. Engstrom, and N. J. Anderson. 2015. Patterns and drivers of change in
417 organic carbon burial across a diverse landscape: Insights from 116 Minnesota lakes.
418 *Global Biogeochemical Cycles* **29**:708-727.
- 419 Dong, X., N. J. Anderson, X. Yang, X. chen, and J. Shen. 2012. Carbon burial by shallow
420 lakes on the Yangtze floodplain and its relevance to regional carbon sequestration.
421 *Global Change Biology* **18**:2205-2217.
- 422 Downing, J. P., M. Meybeck, J. C. Orr, R. R. Twilley, and H. W. Scharpenseel. 1993. Land
423 and water interface zones. *Water, Air, & Soil Pollution* **70**:123-137.
- 424 Enea, A., G. Romanescu, and C. Stoleriu. 2012 Quantitative considerations concerning the
425 source-areas for the silting of the red lake (Romania) lacustrine basin.
426 . Romania.
- 427 Fearnside, P. M. 2005. Do hydroelectric dams mitigate global warming? The case of Brazil's
428 Curuá-Una Dam. *Mitigation and Adaptation Strategies for Global Change* **10**:675-
429 691.

430 Gordon, S. I. 1980. Utilizing LANDSAT imagery to monitor land-use change: A case study
431 in ohio. *Remote Sensing of Environment* **9**:189-196.

432 Goulding, M. 1993. Flooded forests of the Amazon. *Scientific American* **268**:114-120+115.

433 Hoffmann, T., M. Schlummer, B. Notebaert, G. Verstraeten, and O. Korup. 2013. Carbon
434 burial in soil sediments from Holocene agricultural erosion, Central Europe. *Global*
435 *Biogeochemical Cycles* **27**:828-835.

436 INPE. 2016. Program for the Estimation of Amazon Deforestation. Accessed 20 November
437 2016, http://www.obt.inpe.br/prodes/prodes_1988_2015n.htm.

438 Ivanovich, M., and S. Harmon. 1992. Uranium Series Disequilibrium - Applications to Earth,
439 Marine and Environmental Sciences. second edition edition. Oxford Science
440 Publications.

441 Junk, W. J. 2013. Current state of knowledge regarding South America wetlands and their
442 future under global climate change. *Aquatic Sciences* **75**:113-131.

443 Ketterer, M. E., K. M. Hafer, V. J. Jones, and P. G. Appleby. 2004. Rapid dating of recent
444 sediments in Loch Ness: Inductively coupled plasma mass spectrometric
445 measurements of global fallout plutonium. *Science of the Total Environment*
446 **322**:221-229.

447 Ligocki, L. P. 2003. Comportamento geotécnico da barragem de Curuá-Una, Pará. Rio de
448 Janeiro.

449 Lucas, C. M., J. Schöngart, P. Sheikh, F. Wittmann, M. T. F. Piedade, and D. G. McGrath.
450 2014. Effects of land-use and hydroperiod on aboveground biomass and productivity
451 of secondary Amazonian floodplain forests. *Forest Ecology and Management*
452 **319**:116-127.

453 Marotta, H., L. Bento, F. A. De Esteves, and A. Enrich-Prast. 2009. Whole ecosystem
454 evidence of eutrophication enhancement by wetland dredging in a shallow Tropical
455 Lake. *Estuaries and Coasts* **32**:654-660.

456 Marotta, H., C. M. Duarte, F. Meirelles-Pereira, L. Bento, F. A. Esteves, and A. Enrich-Prast.
457 2010. Long-term CO₂ variability in two shallow tropical lakes experiencing episodic
458 eutrophication and acidification events. *Ecosystems* **13**:382-392.

459 Marotta, H., L. Pinho, C. Gudas, D. Bastviken, L. J. Tranvik, and A. Enrich-Prast. 2014.
460 Greenhouse gas production in low-latitude lake sediments responds strongly to
461 warming. *Nature Climate Change* **4**:467-470.

462 Melack, J. M., L. L. Hess, M. Gastil, B. R. Forsberg, S. K. Hamilton, I. B. T. Lima, and E. M.
463 L. M. Novo. 2004. Regionalization of methane emissions in the Amazon Basin with
464 microwave remote sensing. *Global Change Biology* **10**:530-544.

465 Munyati, C. 2000. Wetland change detection on the Kafue Flats, Zambia, by classification of
466 a multitemporal remote sensing image dataset. *International Journal of Remote*
467 *Sensing* **21**:1787-1806.

468 Naidu, A. S., L. W. Cooper, B. P. Finney, R. W. Macdonald, C. Alexander, and I. P.
469 Semiletov. 2000. Organic carbon isotope ratio ($\delta^{13}C$) of Arctic Amerasian
470 Continental shelf sediments. *International Journal of Earth Sciences* **89**:522-532.

471 Neill, C., M. T. Coe, S. H. Riskin, A. V. Krusche, H. Elsenbeer, M. N. Macedo, R.
472 McHorney, P. Lefebvre, E. A. Davidson, R. Scheffler, A. M. e Silva Figueira, S.
473 Porder, and L. A. Deegan. 2013a. Watershed responses to Amazon soya bean
474 cropland expansion and intensification. *Philosophical Transactions of the Royal*
475 *Society B: Biological Sciences* **368**.

476 Neill, C., M. T. Coe, S. H. Riskin, A. V. Krusche, H. Elsenbeer, M. N. Macedo, R.
477 McHorney, P. Lefebvre, E. A. Davidson, R. Scheffler, A. M. Figueira, S. Porder, and
478 L. A. Deegan. 2013b. Watershed responses to Amazon soya bean cropland expansion

479 and intensification. Philosophical transactions of the Royal Society of London. Series
480 B, Biological sciences **368**:20120425.

481 Neue, H. U., J. L. Gaunt, Z. P. Wang, P. Becker-Heidmann, and C. Quijano. 1997. Carbon in
482 tropical wetlands. *Geoderma* **79**:163-185.

483 Ometto, J. P. H. B., J. R. Ehleringer, T. F. Domingues, J. A. Berry, F. Y. Ishida, E. Mazzi, N.
484 Higuchi, L. B. Flanagan, G. B. Nardoto, and L. A. Martinelli. 2006. The stable carbon
485 and nitrogen isotopic composition of vegetation in tropical forests of the Amazon
486 Basin, Brazil. *Biogeochemistry* **79**:251-274.

487 Peixoto, R. B., H. Marotta, D. Bastviken, and A. Enrich-Prast. 2016. Floating Aquatic
488 Macrophytes Can Substantially Offset Open Water CO₂ Emissions from
489 Tropical Floodplain Lake Ecosystems. *Ecosystems* **19**:724-736.

490 Sanders, C. J., B. D. Eyre, I. R. Santos, W. MacHado, W. Luiz-Silva, J. M. Smoak, J. L.
491 Breithaupt, M. E. Ketterer, L. Sanders, H. Marotta, and E. Silva-Filho. 2014. Elevated
492 rates of organic carbon, nitrogen, and phosphorus accumulation in a highly impacted
493 mangrove wetland. *Geophysical Research Letters* **41**:2475-2480.

494 Sanders, C. J., I. R. Santos, D. T. Maher, J. L. Breithaupt, J. M. Smoak, M. Ketterer, M. Call,
495 L. Sanders, and B. D. Eyre. 2016. Examining ²³⁹⁺²⁴⁰Pu, ²¹⁰Pb and historical events
496 to determine carbon, nitrogen and phosphorus burial in mangrove sediments of
497 Moreton Bay, Australia. *Journal of Environmental Radioactivity* **151**:623-629.

498 Sanders, L. M., K. H. Taffs, D. J. Stokes, C. J. Sanders, J. M. Smoak, A. Enrich-Prast, P.
499 Macklin, I. R. Santos, and H. Marotta. 2017. Carbon accumulation in Amazonian
500 floodplain lakes: A significant component of Amazon budgets? *Limnology &
501 Oceanography Letters*:29-35.

502 Skole, D., and C. Tucker. 1993. Tropical deforestation and habitat fragmentation in the
503 amazon: Satellite data from 1978 to 1988. *Science* **260**:1905-1910.

504 Smith, L. K., J. M. Melack, and D. E. Hammond. 2002. Carbon, nitrogen, and phosphorus
505 content and ²¹⁰Pb-derived burial rates in sediments of an Amazon floodplain lake.
506 *Amazoniana* **17**:413-436.

507 Stanley, E. H., S. M. Powers, N. R. Lottig, I. Buffam, and J. T. Crawford. 2012.
508 Contemporary changes in dissolved organic carbon (DOC) in human-dominated
509 rivers: Is there a role for DOC management? *Freshwater Biology* **57**:26-42.

510 Zocatelli, R., P. Moreira-Turcq, M. Bernardes, B. Turcq, R. C. Cordeiro, S. Gogo, J. R.
511 Disnar, and M. Boussafir. 2013. Sedimentary evidence of soil organic matter input to
512 the curuai amazonian floodplain. *Organic Geochemistry* **63**:40-47.

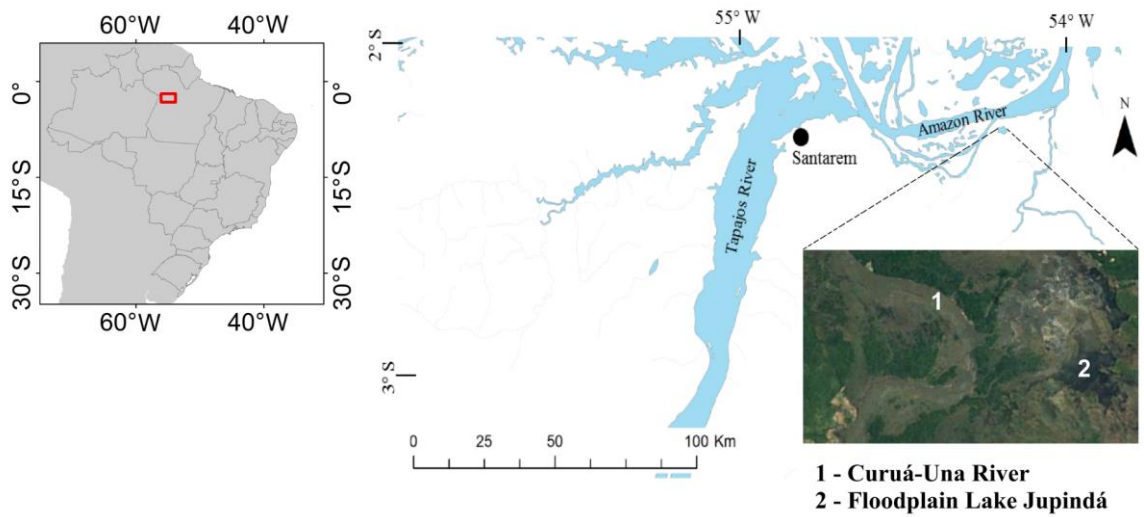
513

514

515

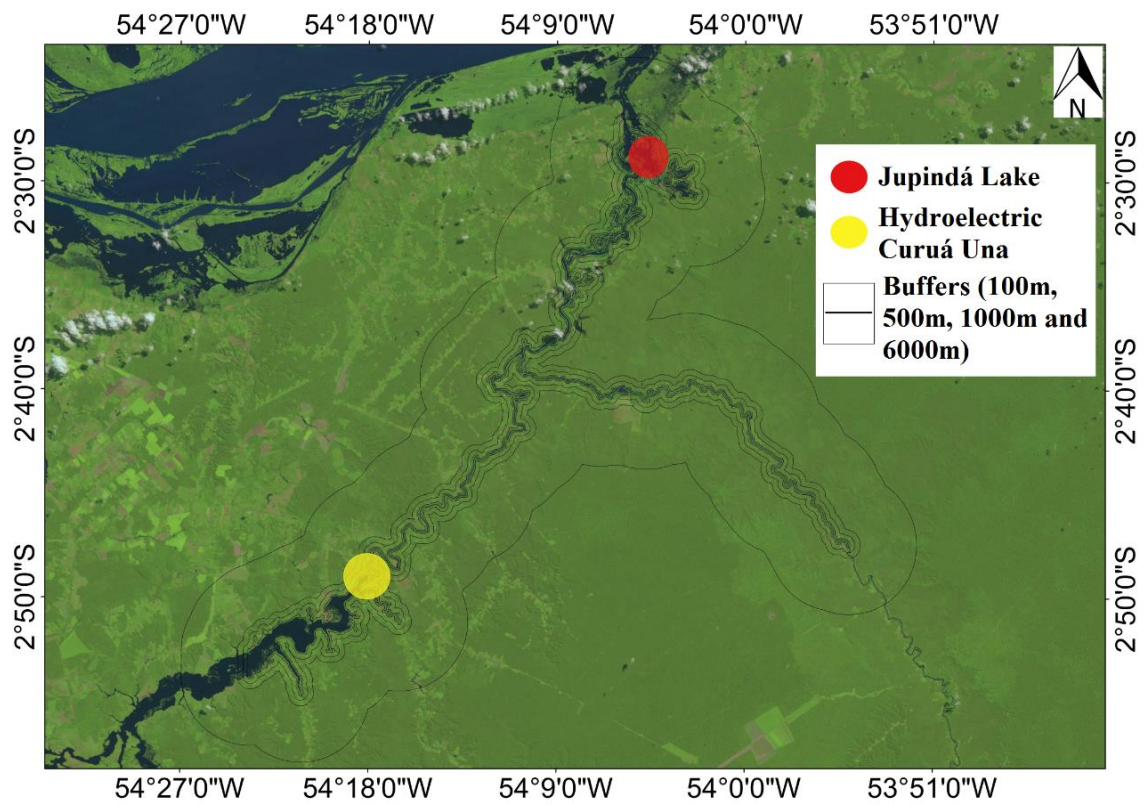
516

517 **Figure 1.**



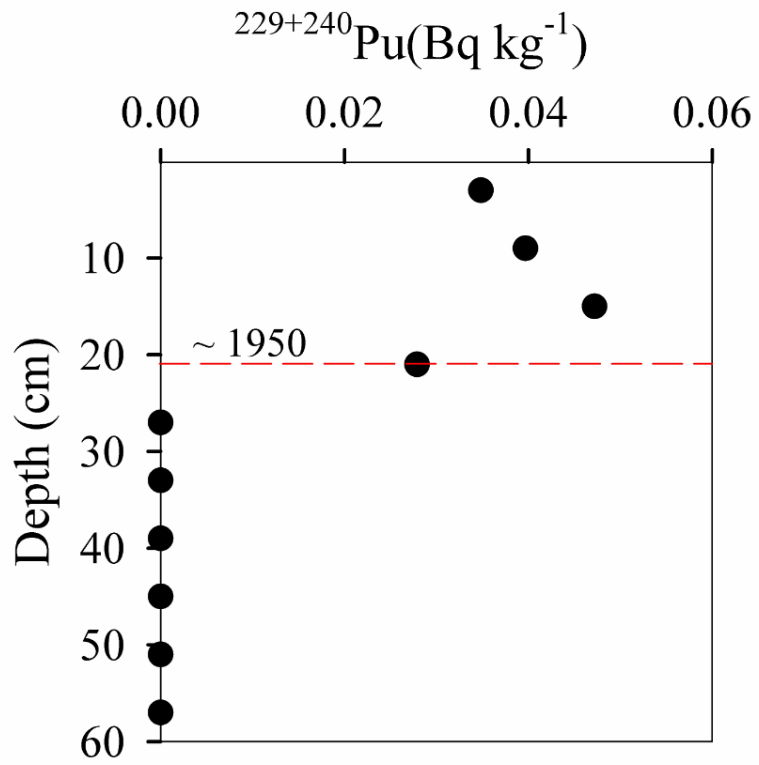
518
 519
 520
 521
 522
 523
 524
 525
 526
 527
 528
 529
 530
 531
 532
 533
 534
 535
 536
 537
 538
 539
 540
 541
 542
 543
 544
 545
 546
 547
 548
 549

Figure 2.



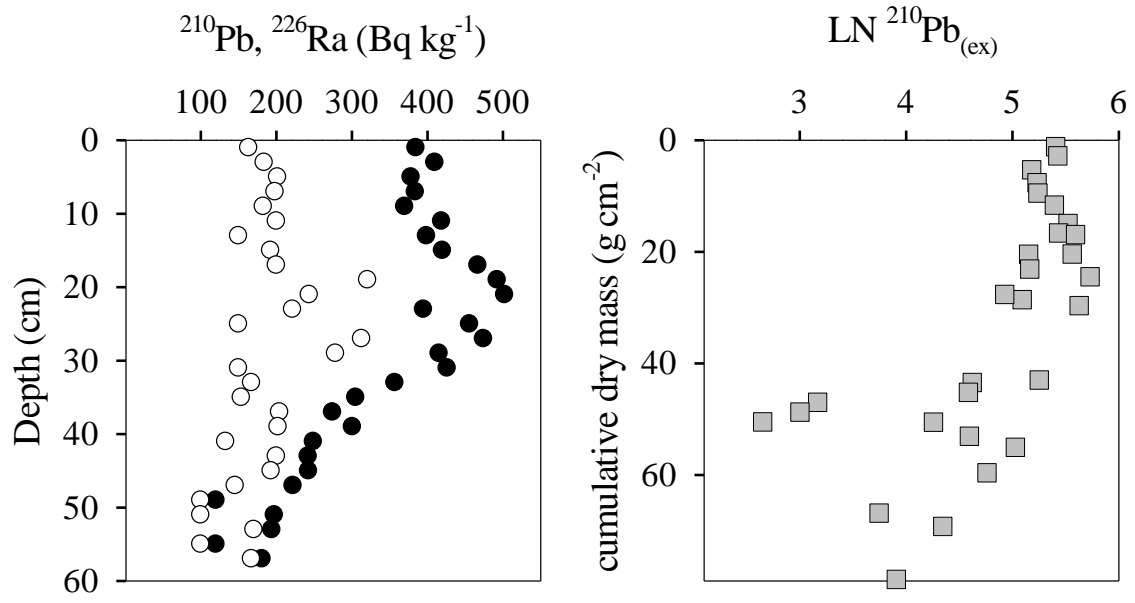
550
551
552
553
554
555
556
557
558
559
560
561
562
563
564
565
566
567
568
569
570
571
572
573
574

Figure 3.



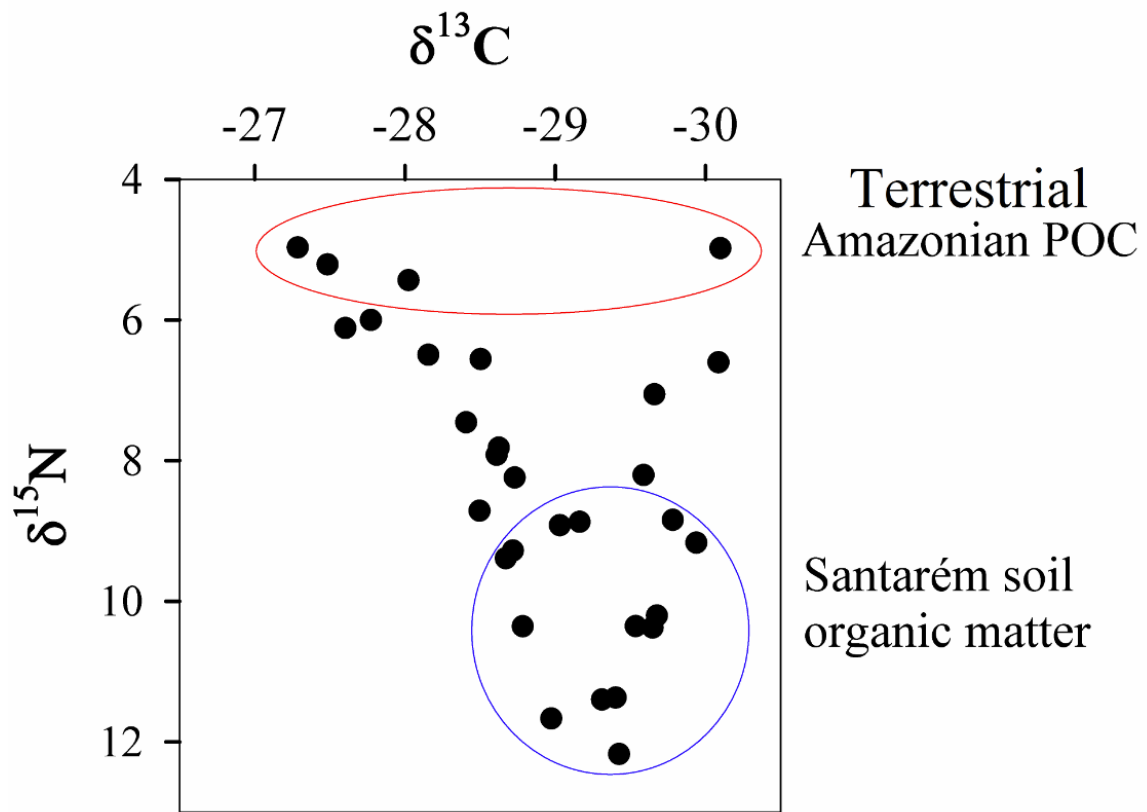
575
 576
 577
 578
 579
 580
 581
 582
 583
 584
 585
 586
 587
 588
 589
 590
 591
 592
 593
 594
 595
 596
 597
 598
 599
 600

Figure 4.



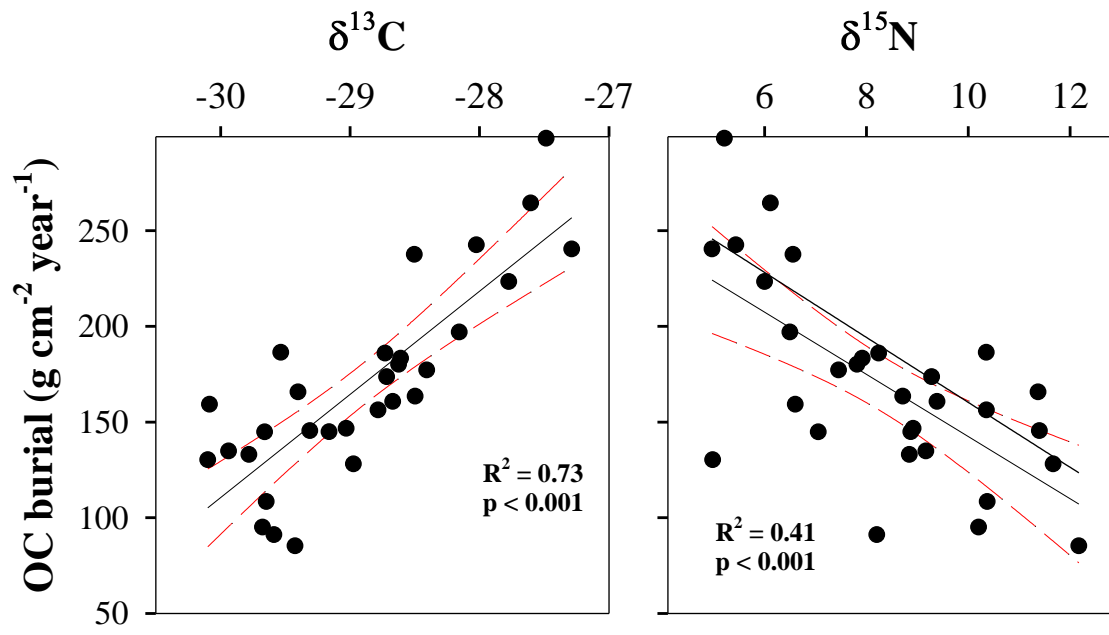
601
 602
 603
 604
 605
 606
 607
 608
 609
 610
 611
 612
 613
 614
 615
 616
 617
 618
 619
 620
 621
 622
 623
 624
 625
 626
 627
 628
 629
 630

Figure 5.



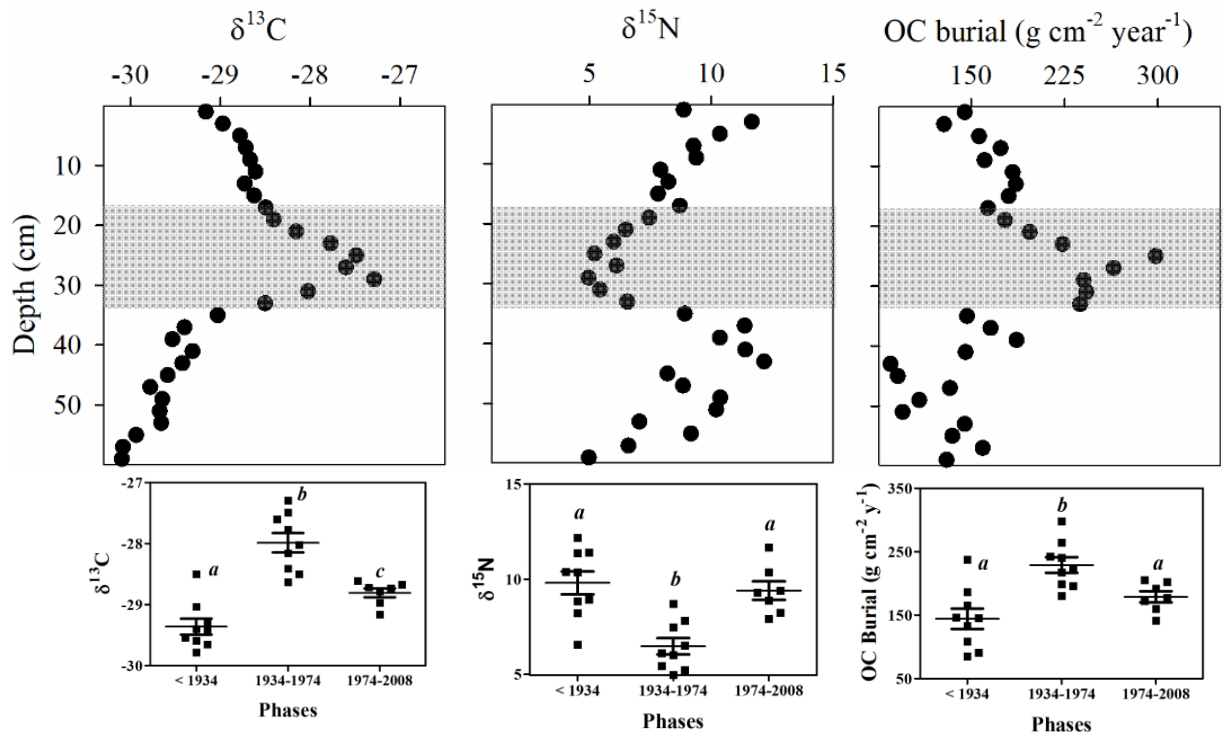
631
 632
 633
 634
 635
 636
 637
 638
 639
 640
 641
 642
 643
 644
 645
 646
 647
 648
 649
 650
 651
 652
 653
 654

Figure 6.



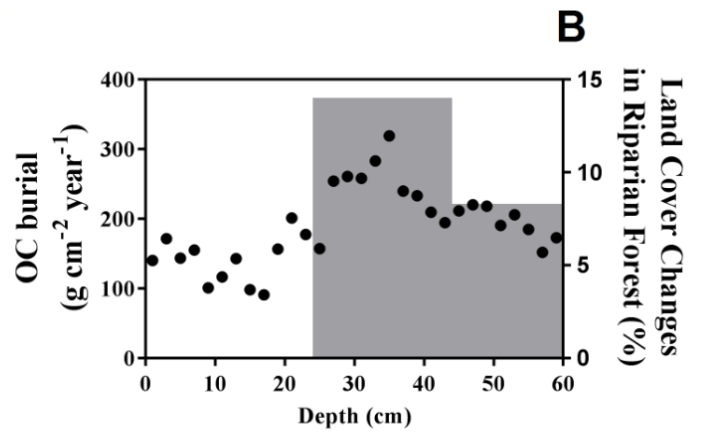
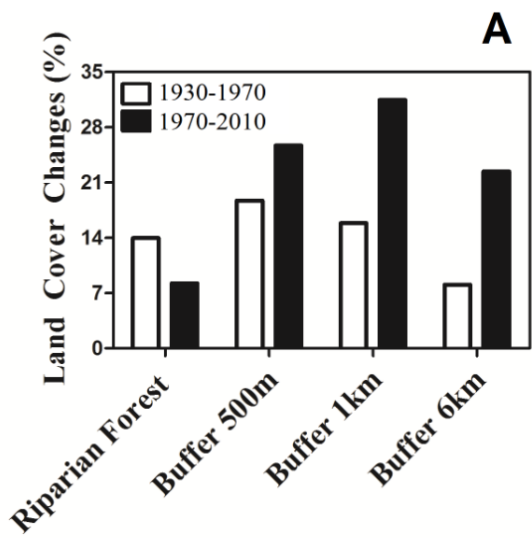
655
 656
 657
 658
 659
 660
 661
 662
 663
 664
 665
 666
 667
 668
 669
 670
 671
 672
 673
 674
 675
 676
 677
 678
 679
 680
 681
 682
 683

Figure 7.



684
685
686
687
688
689
690
691
692
693
694
695
696
697
698
699
700
701
702
703
704
705
706
707
708
709
710

Figure 8.



711
712